Struct Chem
DOI 10.1007/s11224-007-9242-2

ORIGINAL PAPER

Hypervalence and the delocalizing versus localizing propensities of H_3^-, Li_3^-, CH_5^- and SiH_5^-

Simon C. A. H. Pierrefixe · F. Matthias Bickelhaupt

Received: 20 April 2007 / Accepted: 28 April 2007

Abstract Lithium and silicon have the capability to form hypervalent structures, such as Li_3^- and SiH_5^-, which is contrasted by the absence of this capability in hydrogen and carbon, as exemplified by H_3^- and CH_5^- which, although isoelectronic to the former two species, have a distortive, bond-localizing propensity. This well-known fact is nicely confirmed in our DFT study at BP86/TZ2P. We furthermore show that the hypervalence of Li and Si neither originates from the availability of low-energy 2*p* and 3*d* AOs, respectively, nor from differences in the bonding pattern of the valence molecular orbitals; there is, in all cases, a 3-center-4-electron bond in the axial X–A–X unit. Instead, we find that the discriminating factor is the smaller effective size of C compared to the larger Si atom, and the resulting lack of space around the former. Interestingly, a similar steric mechanism is responsible for the difference in bonding capabilities between H and the effectively larger Li atom. This is so, despite the fact that the substituents in the corresponding symmetric and linear dicoordinate H_3^- and Li_3^- are on opposite sides of the central atom.

Keywords Carbon · Density functional calculations · Hydrogen · Hypervalence · Lithium · Silicon

Electronic supplementary material The online version of this article (doi:10.1007/s11224-007-9242-2) contains supplementary material, which is available to authorized users.

S. C. A. H. Pierrefixe · F. M. Bickelhaupt (✉)
Theoretische Chemie, Scheikundig Laboratorium der Vrije Universiteit, De Boelelaan 1083, Amsterdam 1081 HV, The Netherlands
e-mail: FM.Bickelhaupt@few.vu.nl

Introduction

Despite numerous studies, hypervalence in molecular and extended structures continues to be an issue of interest and debate, even to the extent of the meaningfulness of the concept and its very definition, already for about a century [1–5]. Here, we wish to address the different bonding capabilities of the two group-1 atoms H and Li, and two group-14 atoms C and Si. While H usually binds not more than one ligand [6] (except for some examples like the triangular H_3^+), Li, despite being isoelectronic, can bind two or more ligands [7], thus exceeding its formal monovalence and constituting a hypervalent compound. Likewise, C can, in general, bind not more than four ligands [6] (except for some exotic or controversial examples [2, 8, 9a]), whereas its isoelectronic equivalent of the third period, i.e., Si, can bind five [2, 9–11] (or sometimes even six [2, 12]) substituents. The question we want to tackle here is, why lithium and silicon are able to violate their formal mono- and tetravalence, respectively, while hydrogen and carbon do not (or only in rudimentary form) possess this capability?

The nonhypervalence of hydrogen and carbon on one hand, and the hypervalence of lithium and silicon on the other hand, is nicely illustrated by comparing the potential energy surfaces of the corresponding S_N2 reactions, which are of the general form:

$$\begin{aligned} X^- + YX &\rightarrow [X-Y-X^-] \text{ or } [X-Y-X^-]^{\neq} \\ &\rightarrow XY + X^- \end{aligned} \quad (1)$$

In the case of the group-1 atoms hydrogen and lithium, i.e., for X = Y = H or Li, the collinear exchange reaction of H^- + H_2 proceeds via a transition state, while that of Li^- + Li_2 proceeds via a stable transition complex (see also

plain and dotted lines, respectively, in Fig. 1). Thus, although the $D_{\infty h}$ symmetric transition species H_3^- and Li_3^- are isoelectronic and structurally equivalent, H_3^- is a labile species that has the tendency to localize one of its bonds, while Li_3^- is a stable hypervalent equilibrium structure [13–15]. Likewise, in the case of the group-14 atoms carbon and silicon, i.e., for X = H and Y = CH_3 or SiH_3, the hydride exchange reaction of $H^- + CH_4$ proceeds via labile five-coordinate transition state, while that of $H^- + SiH_4$ proceeds via a stable, pentavalent transition complex. Thus, again, although the D_{3h} symmetric species are isoelectronic and show equivalent trigonal bipyramidal geometries, HCH_3H^- is a transition state that tends to localize one of its axial C–H bond, while $HSiH_3H^-$ is a stable transition complex [10, 11, 15–17].

Obviously, hypervalence is of relevance not only in structural chemistry but also in the field of chemical reactivity. Yet, in the present study, we focus rather on the symmetric transition species with a delocalized structure, and on the question of what causes this species to be hypervalent (i.e., stable) or nonhypervalent (i.e., with a tendency to localize one and partially break another bond). These different propensities can also be recognized in the potential energy surfaces depicted in Fig. 1.

Our first objective here is to characterize with density functional theory (DFT), the structures and the energetics of the stationary points in the above-mentioned model systems that involve hypervalently coordinated hydrogen, lithium, carbon, and silicon. To this end, we have conducted an extensive and systematic exploration of the potential energy surface (PES) of HCH_3H^-, $HSiH_3H^-$, H_3^-, and Li_3^-, using the ADF program and the generalized gradient approximation (GGA) of DFT at the BP86/TZ2P level [18].

The main purpose is, however, to obtain a more qualitative, physical insight into the factors that determine *why*

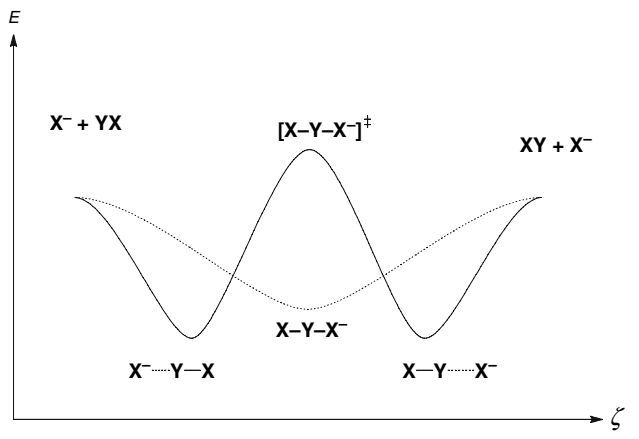

Fig. 1 Double-well (black line) and single-well (dotted line) S_N2 potential energy surfaces of X^- + YX, along the reaction coordinate ζ

Li and Si can form hypervalent species, whereas H and C cannot. The first proposal to elucidate this puzzling problem was Pauling's idea that the hypervalence of the main group atoms in question derives from the availability of low-energy AOs, e.g., *2p* and *3d* in the valence electron shell of lithium and silicon, respectively. However, modern ab initio calculations showed that, for providing bonding in hypervalent species, the central Si and Li atoms predominantly invoke their valence *3s* and *3p* (Si) or *2s* AOs (Li). The low-energy *3d* AOs of silicon merely act as corrective polarization functions, but not as valence orbitals [19]. This is again confirmed in the present study. On the other hand, the low-energy *2p* AOs have been shown to participate more actively in bonding [7b]. Here, we find, however, that their contribution is not essential for the hypervalence in Li_3^-.

Nowadays, the bonding in hypervalent species is described, instead, in terms of the 3-center-4-electron (3c-4e) bond [20]. This model was proposed simultaneously by Pimentel and Rundle [21] to account for the hypervalency of the central atom in species such as F_3^- and XeF_2. The 3c-4e bond was formulated in terms of the valence p_σ atomic orbitals (AOs), of a linear arrangement of three atoms that yields a well-known pattern of three MOs, ψ_1, ψ_2, and ψ_3, similar to those shown in Scheme 1, left panel, which are bonding, nonbonding, and antibonding, respectively, with the four electrons in ψ_1 and ψ_2 [22]. A similar formulation in terms of the valence *s* orbitals was later introduced to account for the bonding in species like H_3^-, see Scheme 1 right panel.

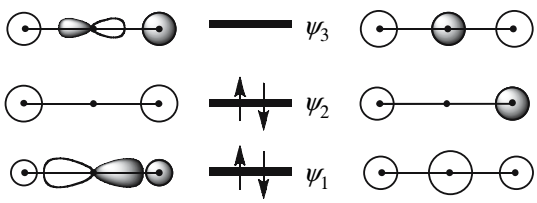

Scheme 1 Frontier orbitals involved in 3c-4e bonding with central *p* orbitals (left panel) and with central *s* orbitals (right panel)

Note that, whereas the 3c-4e MO model accounts for the bonding in hypervalent species, it does *not* explain *why*, for example, silicon and lithium can accommodate more ligands in their valence shell than carbon and hydrogen respectively. Indeed MO theory has so far not elucidated why similar bonding mechanisms (i.e. the 3c-4e bonds) yield, in some cases, labile species, such as H_3^- and CH_5^-, and in other cases stable minima as, for example, Li_3^- and SiH_5^-. Here we anticipate that our analyses highlight, in agreement with early work by Schleyer, Dewar or Gillespie [4, 11, 23], that steric factors are important for understanding the hypervalency of SiH_5^- and nonhypervalency of CH_5^-. Interestingly, steric factors also appear to be

responsible to account for the hypervalency of Li_3^-, as opposed to the nonhypervalency of H_3^-, even though the central atom in the latter species is only two-coordinate.

Theoretical methods

All calculations were performed using the Amsterdam Density Functional (ADF) program developed by Baerends and others [18]. The numerical integration was performed using the procedure developed by te Velde et al. [18g, h]. The MOs were expanded in a large uncontracted set of Slater-type orbitals (STOs) containing diffuse functions: TZ2P (no Gaussian functions are involved) [18i]. The basis set is of triple-ζ quality for all atoms, and has been augmented with two sets of polarization functions, i.e. 3*d* and 4*f* on C and Li, 4*d* and 5*f* on Si and 2*p* and 3*d* on H. The 1*s* core shell of carbon and lithium, and the 1*s*2*s*2*p* core shell of silicon were treated by the frozen-core approximation [18c]. An auxiliary set of *s*, *p*, *d*, *f*, and *g* STOs was used to fit the molecular density, represent the Coulomb, and exchange potentials accurately in each self-consistent field cycle [18j].

Equilibrium structures were optimized using analytical gradient techniques [18k]. Geometries, energies, and vibrational frequencies were computed at the BP86 level of the generalized gradient approximation (GGA): exchange is described by Slater's Xα potential [18l] with corrections due to Becke [18m, n] added self-consistently and correlation is treated in the Vosko-Wilk-Nusair (VWN) parameterization [18o] with nonlocal corrections due to Perdew [18p] added, again, self-consistently (BP86) [18q].

Results and discussion

Structures and relative energies

Initially, we focus on the geometries and relative energies of the various XYX^- species, computed at the BP86/TZ2P level of theory, which are collected in Fig. 2. Note that Fig. 2 shows relative energies of any XYX^- relative to $X^- + YX$. In line with previous work (see introduction), the D_{3h} symmetric five-coordinate CH_5^- (**1a**), which has two equivalent C–H bonds of 1.68 Å, is a first-order saddle-point. It has the propensity to localize one C–H bond to 1.10 Å, and stretch the other C–H bond to 3.83 Å, yielding $H^-\cdots CH_4$ (**1b**) in C_{3v} symmetry. Whereas the five-coordinate **1a** is 40 kcal/mol above separate $H^- + CH_4$, the localized **1b** is at about –1 kcal/mol (see Fig. 2). We note that **1b** is not the global minimum, but a second-order saddle point with two imaginary frequencies that are associated with the $H^-\cdots$C–H bending mode. The real minimum is constituted by a C_s symmetric $H^-\cdots CH_4$ species at –3.55 kcal/mol in which, the hydride anion forms a hydrogen bond with one of the methane C–H bonds, to a slightly deformed methane weakly bound to the hydrogen anion via one of the hydrogen of the methane (not shown in Fig. 2).

At variance with the carbon species **1a**, the D_{3h} symmetric five-coordinate SiH_5^- (**2a**), which has two equivalent Si–H bonds of 1.64 Å, is a stable equilibrium structure without any labile, distortive mode (see Fig. 2). This pentavalent **2a** species is at –27 kcal/mol relative to the separate $H^- + SiH_4$.

The group-1 atoms H and Li in A_3^- structures show a similar behavior as the group-14 central atoms in AH_5^-. Thus, the $D_{\infty h}$ symmetric dicoordinate H_3^- (**3a**), which has two equivalent H–H bonds of 1.08 Å, is a first-order saddle-point with the propensity to distort toward a localized $C_{\infty v}$ symmetric $H^-\cdots H_2$ (**3b**) structure with a short and a long H–H bond of 0.78 and 2.35 Å, respectively (see Fig. 2). We find the dicoordinate **3a** at 1 kcal/mol above, and the localized **3b** at –3 kcal/mol relative to separate $H^- + H_2$. At variance, the $D_{\infty h}$ symmetric dicoordinate Li_3^- (**4a**), which has two equivalent Li–Li bonds of 3.05 Å is a stable, hypervalent species at –22 kcal/mol relative to separate $Li^- + Li_2$ (see Fig. 2).

In conclusion, all structural trends and features in potential energy surfaces computed here agree satisfactorily with earlier experimental and theoretical studies [10, 11, 13–17].

Role of silicon 3*d* and lithium 2*p* AOs

As pointed out in the introduction, our analyses show that the availability of low-energy 3*d* and 2*p* AOs in silicon and lithium, respectively, is not responsible for the capability of these atoms to form hypervalent structures. This insight emerges from computations in which we removed the 2*p* orbitals of lithium, and the 3*d* orbitals of silicon from the respective basis sets. The net effect of deleting these low-energy AOs is destabilization of Li_3^- and SiH_5^- by 1.56 and 7.74 kcal/mol, respectively, relative to the separate reactants (not shown in Fig. 2). Importantly, however, both Li_3^- and SiH_5^- remain stable hypervalent equilibrium structures. The deletion of the low-energy 2*p* and 3*d* AOs does not lead to a distortive, bond localizing propensity. The only effect is the elongation in axial bond lengths compared to the computation with the full basis set. Thus, the Li–Li bonds in Li_3^- expand by 0.1038 Å compared to **4a**. The axial Si–H bonds in SiH_5^- expand by 0.0247 Å compared to **2a,** while the equatorial Si–H bonds are more or less unaffected (1.5401 Å compared to 1.5428 in **2a**). Thus, in line with previous work on other hypervalent compounds

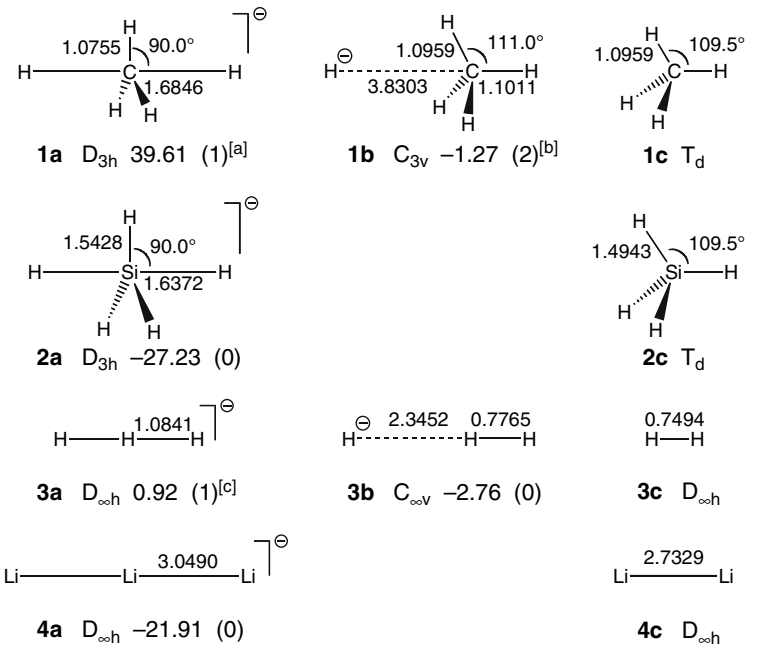

Fig. 2 Geometries (in Å, deg.), energies relative to reactants X^- + YX (in kcal/ mol, see also Eq. 1), and number of imaginary frequencies (in parentheses) of selected species involved in bonding at C, Si, H, and Li (i.e., **1**, **2**, **3,** and **4**, respectively), computed at BP86/TZ2P. [a] i1234 cm^{-1}. [b] i123 cm^{-1}. [c] i1083 cm^{-1}

[19], we find that although the low-energy 2*p* orbitals of lithium and the 3*d* orbitals of silicon are important for a correct quantitative description, they are not responsible for the hypervalence of the these atoms. Note that somewhat larger geometry effects in the case of Li 2*p* deletion compared to Si 3*d* deletion are in line with the earlier finding that lithium 2*p* AOs participate more actively in bonding [7b].

Analysis of CH_5^- versus SiH_5^-

The question remains, what *does* cause the difference in bonding capabilities between, on one hand, H and C and, on the other hand, Li and Si. Our analyses of the orbital electronic structure show that there are also no qualitative differences in terms of the presence or absence of 3c-4e bonding: this bonding pattern occurs pronouncedly in all four symmetric species, i.e., CH_5^- and SiH_5^- (Scheme 1, left), and H_3^- and Li_3^- (Scheme 1, right).

The origin of the difference in bonding capabilities between C and Si in CH_5^- and SiH_5^-, respectively, appears to be related to the effective size of the central atom and the question if there is sufficient space to bind more than four substituents. A first indication for such steric mechanism is much larger expansion of the C–H bond in the trigonal bipyramidal CH_5^- (**1a**) compared to CH_4 (**1c**), namely, by 0.59 Å, than that of the Si–H bond in SiH_5^- (**2a**) compared to SiH_4 (**2c**), which amounts to only 0.14 Å (see Fig. 2).

This observation has inspired us to explore if removal of the steric bulk associated with the equatorial H substituents in CH_5^- (**1a**) would stabilize the resulting linear H–C–H anion

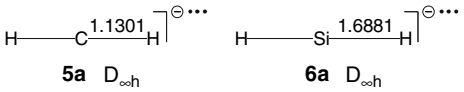

Fig. 3 Geometries (in Å) of H–C–$H^{-\bullet\bullet\bullet}$ (**5a**) and H–Si–$H^{-\bullet\bullet\bullet}$ radicals (**6a**), computed at BP86/TZ2P

and, possibly, make it an equilibrium structure. Note that this species must be a triradical in order to have it in the valence state, that this moiety possesses in **1a**. Strikingly, this is exactly what happens as can be seen in Fig. 3. The optimized geometry of H–C–$H^{-\bullet\bullet\bullet}$ is indeed stable with respect to bond localization. If we optimize H–C–$H^{-\bullet\bullet\bullet}$ in $C_{\infty v}$ symmetry the resulting species **5a** has two equivalent C–H bonds of 1.13 Å, nearly of the same length (only 0.03 Å longer) as those in CH_4 (**1c**).[1] This agrees well with the idea that by going from five- to two-coordination, we have created sufficient space around carbon to accommodate the remaining H substituents in a stable fashion. The removal of the equatorial H substituents from SiH_5^- (**2a**) does not lead to a reduction of the Si–H bond length, in line with the picture that the larger silicon atom already had sufficient space to accommodate all five H substituents in **2a**. The resulting $D_{\infty h}$ symmetric H–Si–$H^{-\bullet\bullet\bullet}$ (**6a**) remains stable with respect to bond length alternation, and the Si–H bonds are even slightly (i.e., 0.05 Å) longer than in SiH_5^- (**2a**) (see Fig. 3).

The above results support the "steric model" of (non)hypervalence in which, the five H substituents,

[1] Whereas **5a** is stable with respect to C–H bond localization, it is labile with respect to H–C–H bending. The C_{2v} symmetric equilibrium structure is 2.06 kcal/mol more stable than **5a**, has an H–C–H angle of 142°, and C–H bonds of 1.12 Å, essentially the same as in **5a**.

especially along the axial direction, can not simultaneously approach the small carbon atom "sufficiently" close, i.e., they can not adopt an intrinsically (close-to) optimal C–H distance. This picture gains further support from the following numerical experiments. If CH_5^- (**1a**) is labile due to too long, especially axial C–H bonds, then simply displacing the central C atom along the molecular axis toward one of the axial hydrogen atoms *in an otherwise frozen H_5 structure* (i.e., the five hydrogen substituents retain their relative positions as in **1a**), should cause a similar energy lowering, as allowing CH_5^- (**1a**) to fully relax toward $H^-\cdots CH_4$ (**1b**). As shown in Fig. 4a, this is again exactly what happens. Note that the energy of SiH_5^-, as one might expect, *increases* if we carry out the corresponding numerical experiment of moving the central Si atom of **2b** toward an axial hydrogen atom, while keeping the five hydrogen atoms frozen to their geometry in **2b** (see Fig. 4a).

The same numerical experiments as shown in Fig. 4a have also been carried out in the absence of the equatorial H substituents, i.e., for $H–C–H^{-\bullet\bullet\bullet}$ and $H–Si–H^{-\bullet\bullet\bullet}$ species with frozen H^{axial}–H^{axial} distances taken from **1a** and **2a**, respectively (see Fig. 4b). As can be seen, the change in energy of these $H–C–H^{-\bullet\bullet\bullet}$ and $H–Si–H^{-\bullet\bullet\bullet}$ species (Fig. 4b) closely resembles that of the corresponding ones *with* the three equatorial H atoms (Fig. 4a). This suggests that as the CH_5^- species cannot accommodate all five H substituents at sufficiently short H distances, stabilization can be achieved by partially breaking ("giving up") one of the anyway too long axial C–H bonds, and to localize the other one, yielding net stabilization. This is not necessary in SiH_5^-, because here all Si–H bonds are already relatively close to their intrinsic optimum, and localization rather destabilizes the system.

Analysis of H_3^- versus Li_3^-

Thus, steric overcrowding around the smaller carbon atom in five-coordinate CH_5^- (**1a**) prevents the latter from being stable, as opposed to the stable hypervalent SiH_5^- (**2a**), in which there is sufficient room around the larger silicon atom. Could such steric arguments also explain the difference in bonding capabilities between H_3^- and Li_3^-? This seems not so plausible, at first sight, because the two terminal substituents in these species (**3a** and **4a** in Fig. 2) are on opposite sides of the central atom, and one might therefore expect that they are never in steric contact.

Strikingly, however, we find that steric factors make the difference between the nonhypervalent H_3^- and hypervalent Li_3^-. In the first place, the expansion of the H–H bond in the symmetric H_3^- (**3a**) compared to H_2 (**3c**) is larger than that of the Li–Li bond in Li_3^- (**4a**) compared to Li_2 (**4c**) (see Fig. 2). Note that, whereas in absolute numbers the bond-length expansions seem to be not so different, i.e., +0.33 versus +0.32 Å, respectively, these values correspond to an elongation by +45% for the H–H bond in **3a** compared to the much smaller expansion of +12% for the Li–Li bond in **4a**. This difference in behavior between H_3^- and Li_3^- is strongly reminiscent of the corresponding differences between CH_5^- and SiH_5^-.

To further reveal the origin of the destabilization and H–H bond elongation in H_3^- (**3a**), we have scanned the potential energy surface as a function of a symmetric variation of both H–H bond distances, i.e., $D_{\infty h}$ symmetry is preserved. In Fig. 5a, one can see how the energy of H_3^- rises if, proceeding from the stationary point **3a**, the H–H distances decrease or increase. This is not unexpected, of course, and exactly the same happens in the analogous numerical experiment with Li_3^- (see Fig. 5b). It becomes interesting, however, if we decompose this net energy into two steps, corresponding with bringing together first the terminal substituents in $[A\cdots A]^{-\bullet}\cdot$ (see Eq. 2) followed by the assembly of these substituents and the central atom $A^\bullet$ to yield the overall A_3^- species (see Eq. 3, A = H, Li):

$$A^- + A^\bullet \rightarrow [A\cdots A]^{-\bullet} \tag{2}$$

$$[A\cdots A]^{-\bullet} + A^\bullet \rightarrow [A-A-A]^- \tag{3}$$

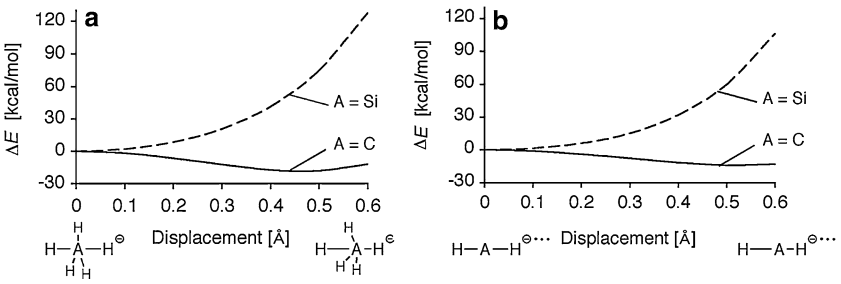

Fig. 4 Energy relative to the symmetric structure, (**a**) for $H–CH_3–H^-$ and $H–SiH_3–H^-$ and (**b**) for $H–C–H^{-\bullet\bullet\bullet}$ and $H–Si–H^{-\bullet\bullet\bullet}$, as a function of the displacement of the central atom A along the main symmetry axis toward an axial H substituent in the otherwise frozen $H–H_3–H$ (**a**) and H···H moiety (**b**), computed at BP86/TZ2P

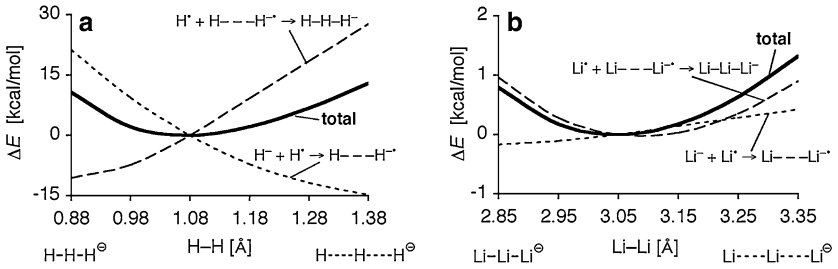

Fig. 5 Energy of $D_{\infty h}$ symmetric H–H–H$^-$ (**a**) and Li-Li-Li$^-$ (**b**) relative to the transition state (**3a**) and stable transition complex (**4a**) structures, respectively, as a function of the A–A distance (A = H or Li), computed at BP86/TZ2P. The relative energies (bold lines, designated "total") are decomposed as indicated by the partial reactions (see also text)

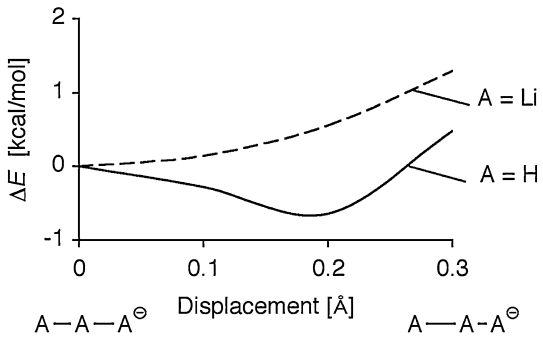

Fig. 6 Energy relative to the symmetric structure for H–H–H$^-$ and Li–Li–Li$^-$ as a function of the displacement of the central atom A (=H or Li) along the main symmetry axis toward an axial A substituent in the otherwise frozen A···A moiety, computed at BP86/TZ2P

As can be clearly seen in Fig. 5a, the energy of $D_{\infty h}$ symmetric H_3^- as a function of the H–H distance is the result of a trade-off at H–H = 1.08 Å between, on one hand, minimizing by H–H expansion, the repulsive energy of the moiety of the outer substituents $[H\cdots H]^{-\bullet}$ and, on the other hand, maximizing by H–H contraction, the bonding with the central H atom. Clearly, the outer H substituents in H_3^- (**3a**) are in steric contact and repel each other.

The above situation for H_3^- differs dramatically from the one of Li_3^-, which is shown Fig. 5b. Here, the energy curve for the moiety of the outer substituents $[Li\cdots Li]^{-\bullet}$ is very shallow. Note that, in fact it is even slightly attractive at the equilibrium Li–Li distance of 3.05 Å in **4a** (see Fig. 5b). This is at variance with the $[H\cdots H]^{-\bullet}$ curve, which is pronouncedly repulsive around the H–H optimum in H_3^- (see Fig. 5a). Thus, the terminal Li substituents in Li_3^- (**4b**) only weakly interact. The driving force for the optimum Li–Li distance is predominantly the Li–Li bonding between the terminal substituents $[Li\cdots Li]^{-\bullet}$ and the central $Li^{\bullet}$ atom (see Fig. 5b).

Thus, the direct repulsion between the terminal H atoms in H_3^- prevents them from coming sufficiently close to the central H atom. In line with this picture, displacing the central H atom in H_3^- (**3a**) toward one of the H substituents (while keeping the geometry of the outer substituents frozen to that in **3a**) causes one strong H–H bond to be formed, which indeed goes with a stabilization of the system (see Fig. 6). A similar displacement of the central Li atom in Li_3^- (**4a**) yields instead a destabilization, as one might expect. This difference in behavior between H_3^- and Li_3^- is reminiscent of the difference in behavior between CH_5^- and SiH_5^-, described above.

Finally, in accordance with the steric model developed above, if we replace the central H atom in H_3^- (**3a**) by the larger Li atom, a stable $D_{\infty h}$ symmetric H–Li–H$^-$ species results. This H–Li–H$^-$ species has two equivalent Li–H bonds of 1.75 Å, and is at –55.74 kcal/mol with respect to separate H$^-$ + LiH (data not shown in the figures). The distance between the outer hydrogen substituents in H–Li–H$^-$ (3.50 Å) is significantly larger than that in H_3^- (**3a**: 2.17 Å). Consequently, the outer hydrogens in H–Li–H$^-$ are (at variance to the situation of **3a**) not in steric contact, and thus a stable hypervalent species can occur.

Conclusions

The hypervalence of lithium and silicon as opposed to the nonhypervalence of the isoelectronic hydrogen and carbon atoms (exemplified in this theoretical study by Li_3^-, SiH_5^-, H_3^-, and CH_5^-, respectively) is shown to neither originate from the availability of low-energy 3*d* and 2*p* AOs, respectively, nor from differences in the bonding pattern of the valence molecular orbitals. In all model species analyzed, we find the 3-center-4-electron bonding pattern in the axial X–A–X unit. We show that instead the discriminating factor is the smaller effective size of C compared to the larger Si atom and the resulting lack of space around the former.

Interestingly, a similar steric mechanism appears to be responsible for the difference in bonding capabilities between H and the effectively larger Li atom. This may seem remarkable because of the fact that the substituents in the corresponding symmetric and linear dicoordinate H_3^- and Li_3^- are on opposite sides of the central atom, seemingly

out of each others way. However, the small effective size of hydrogen causes very short H–H bonds in H_3^-. This, in turn, yields a short mutual distance, less than 2.2 Å, between the terminal H atoms which, therefore, are in steric contact. The terminal Li atoms in Li_3^-, on the other hand, are separated by 6.1 Å and have virtually no steric contact.

Acknowledgment We thank the Netherlands Organization for Scientific Research (NWO-CW and NWO-NCF) for financial support.

References

1. Lewis GN (1916) J Am Chem Soc 38:762
2. Akiba KY (1998) Chemistry of hypervalent compounds. Wiley-VCH, New York
3. (a) Hoffmann R (1989) Solids and surfaces: a chemist's view of bonding in extended structures. John Wiley & Sons Inc, New York; (b) Musher JI (1969) Angew Chem Int Ed Engl 8:54; (c) Pauling L (1960) The nature of the chemical bond. Cornell University Press, Ithaca, New York
4. (a) Noury S, Silvi B, Gillespie RJ (2002) Inorg Chem 41:2164; (b) Gillespie RJ, Robinson EA (1995) Inorg Chem 34:978
5. Cioslowski J, Mixon ST (1993) Inorg Chem 32:3209
6. (a) Smith MB, March J (2001) Advanced organic chemistry: reactions, mechanisms and structure. Wiley-Interscience, New York; (b) Carey FA, Sundberg RJ (2000) Advanced organic chemistry: structure and mechanisms (Part A). Springer, New York; (c) Streitwieser A, Heathcock CH, Kosower EM (1998) Introduction to organic chemistry. Prentice Hall, Paramus
7. (a) Jones RO, Lichtenstein A, Hutter JJ (1997) Chem Phys 106:4566; (b) Bickelhaupt FM, Hommes N, Fonseca Guerra C, Baerends EJ (1996) Organometallics 15:2923; Bickelhaupt FM, Solà M, Fonseca Guerra C (2006) J Chem Theory Comput 2:965
8. (a) Akiba K, Yamashita M, Yamamoto Y, Nagase S (1999) J Am Chem Soc 121:10644; (b) Olah GA, Prakash GKS, Williams RE, Field LD, Wade K (1987) Hypercarbon chemistry. John Wiley & Sons Inc, New York; (c) Forbus TR, Martin JC (1979) J Am Chem Soc 101:5057
9. (a) Martin JC (1983) Science 221:509; (b) Bento AP, Bickelhaupt FM (2007) J Org Chem 72:2201; (c) Bento AP, Solà M, Bickelhaupt FM (2005) J Comput Chem 26:1497
10. (a) Hajdasz DJ, Squires RR (1986) J Am Chem Soc 108:3139; (b) Wilhite DL, Spialter L (1973) J Am Chem Soc 95:2100; (c) Keil F, Ahlrichs R (1975) Chem Phys 8:384; (d) Hajdasz DJ, Ho YH, Squires RR (1994) J Am Chem Soc 116:10751
11. Reed AE, Schleyer PVR (1987) Chem Phys Lett 133:553
12. (a) Gutsev GL (1991) Chem Phys Lett 184:305; (b) Hamilton WC (1962) Acta Crystallographica 15:353
13. (a) Kabbaj OK, Lepetit MB, Malrieu JP, Sini G, Hiberty PC (1991) J Am Chem Soc 113:5619; (b) Kabbaj OK, Volatron F, Malrieu JP (1988) Chem Phys Lett 147:353; (c) Braida B, Hiberty PC (2004) J Am Chem Soc 126:14890
14. (a) Michels HH, Montgomery JA (1987) Chem Phys Lett 139:535; (b) Starck J, Meyer W (1993) Chem Phys 176:83
15. Keil F, Ahlrichs R (1976) J Am Chem Soc 98:4787
16. (a) Baybutt P (1975) Mol Phys 29:389; (b) Carroll MT, Gordon MS, Windus TL (1992) Inorg Chem 31:825; (c) Ritchie CD, Chappell GA (1970) J Am Chem Soc 92:1819; (d) Dedieu A, Veillard A (1972) J Am Chem Soc 94:6730; (e) Payzant JD, Tanaka K, Betowski LD, Bohme DK (1976) J Am Chem Soc 98:894; (f) Shi Z, Boyd RJ (1991) J Phys Chem 95:4698
17. (a) Sini G, Hiberty PC, Shaik SS (1989) J Chem Soc, Chem Comm 772; (b) Sini G, Ohanessian G, Hiberty PC, Shaik SS (1990) J Am Chem Soc 112:1407
18. (a) te Velde G, Bickelhaupt FM, Baerends EJ, Fonseca Guerra C, van Gisbergen SJA, Snijders JG, Ziegler T (2001) J Comput Chem 22:931; (b) Fonseca Guerra C, Visser O, Snijders JG, te Velde G, Baerends EJ (1995) Parallelization of the Amsterdam Density Functional Programme. In: Clementi E, Corongiu G (eds) Methods and techniques for computational chemistry. STEF, Cagliari, 305 pp; (c) Baerends EJ, Ellis DE, Ros P (1973) Chem Phys 2:41; (d) Baerends EJ, Ros P (1975) Chem Phys 8:412; (e) Baerends EJ, Ros P (1978) Int J Quantum Chem 169; (f) Fonseca Guerra C, Snijders JG, te Velde G, Baerends EJ (1998) Theor Chem Acc 99:391; (g) Boerrigter PM, te Velde G, Baerends EJ (1988) Int J Quantum Chem 33:87; (h) te Velde G, Baerends EJ (1992) J Comput Phys 99:84; (i) Snijders JG, Baerends EJ, Vemooijs P (1982) At Nucl Data Tables 26:483; (j) Krijn J, Baerends EJ (1984) Fit-functions in the HFS-method; internal report (in Dutch), Vrije Universiteit; (k) Versluis L, Ziegler TJ (1988) Chem Phys 88:322; (l) Slater JC (1974) Quantum theory of molecules and solids, vol 4. McGraw-Hill, New-York; (m) Becke AD (1986) J Chem Phys 84:4524; (n) Becke AD (1988) Phys Rev A 38:3098; (o) Vosko SH, Wilk L, Nusair M (1980) Can J Phys 58:1200; (p) Perdew JP (1986) Phys Rev B 33:8822; 34:7406; (q) Fan LY, Ziegler T (1991) J Chem Phys 94:6057
19. (a) Kutzelnigg W (1984) Angew Chem Int Ed Engl 23:272; (b) Magnusson E (1990) J Am Chem Soc 112:7940; (c) Reed AE, Schleyer PVR (1990) J Am Chem Soc 112:1434; (d) Bickelhaupt FM, Sola M, Schleyer PVR (1995) J Comput Chem 16:465
20. Hoffmann R, Howell JM, Muetterties EL (1972) J Am Chem Soc 94:3047
21. (a) Pimentel GC (1951) J Chem Phys 19:446; (b) Hach RJ, Rundle RE (1951) J Am Chem Soc 73:4321
22. (a) Landrum GA, Goldberg N, Hoffmann R (1997) J Chem Soc, Dalton Trans 3605; (b) Ramsden CA (1994) Chem Soc Rev 23:111; (c) Albright TA, Burdett JK, Whangbo M-H (1985) Orbital interactions in chemistry. John Wiley & Sons Inc, New York
23. Dewar MJS, Healy E (1982) Organometallics 1:1705